Active Magnetic Support and Design of High Speed Rotors for Powerful Electric Drives

F. VIGGIANO AND G. SCHWEITZER

ABSTRACT

The main topic of this project is to develop the scientific basis and the technology for the design of electric high speed power drives. This paper describes the main conclusions on the design, the modeling and the control of the magnetically supported high speed rotor. First results on a realized prototype high speed drive with 100 KW power at 30'000 RPM will be presented.

INTRODUCTION

The development of magnetic bearings and power-electronics has considerably facilitated the realization of fast and powerful electric drives. Especially for pumps and compressors such drives have significant technical and economical advantages. Since the power concentration of a machine rises with its rotational speed, the machine will become smaller. In addition, mechanical gears between drive and load are no more necessary and so the whole lubrication circuit for gears as well as for bearings can be avoided. The use of modern inverters for the motor power supply finally allows a variable operating-speed adjustment and an optimal process-utilization. The main objective of a project sponsored by the Swiss Federal Institute of Technology (ETH) is to develop the scientific basis and the technology for the design of high speed power drives in a range of 100 KW - 5 MW power and up to 30'000 RPM. The following Institutes within the Mechatronics Lab are cooperating in this project: *Inst. of Electrical Machines, Inst. of El'technical Development and Design, and Inst. of Robotics*. In order to verify this direct drive concept and to make practical experience, a prototype with 100 KW power and with a rotational speed of 30'000 RPM has been realized. The active magnetic support and the design of the high speed rotor is the main topic discussed in this paper.

LIMITS OF ROTOR-DESIGN FOR ELECTRIC HIGH SPEED DRIVES

The induction machine with squirrel-cage is the most suited type of electrical machine for high speed applications (Figure 1). This is because the induction machine is very simple from the point of view of construction, and furthermore no brushes for the current collection are necessary. However, the design of the rotor of a high speed induction machine, as shown in Figure 1, still is a very demanding task. Not only electrical requirements have to be fulfilled, but additionally mechanical considerations gain in importance with increasing rotational speeds. One of the most crucial parameters of the motor design is the driving power. From a user point of view the motor should obviously achieve a prescribed power output P which can be related to geometric and frequency parameters [6]:

F. Viggiano and G. Schweitzer, Mechatronics Lab, Swiss Federal Institute of Technology (ETH), 8092 Zurich, Switzerland

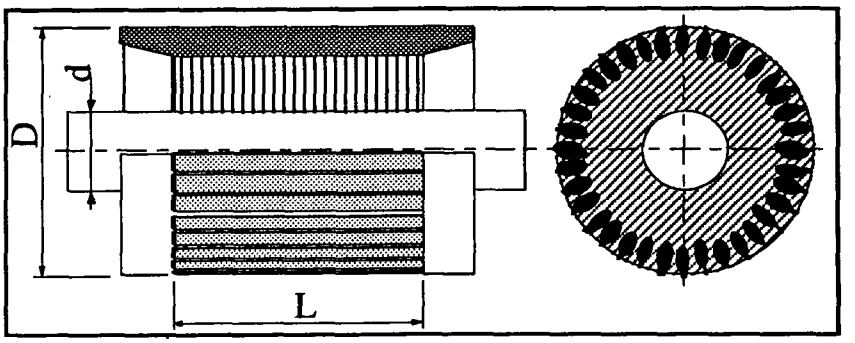

Figure 1: Rotor of a laminated induction machine with squirrel-cage

$$P \leq C\, L\, D^2 f / p \tag{1}$$

In equation (1) C is the utilization factor of the machine, L the motor length, D the rotor diameter, f the stator frequency and p the number of pole pairs. Equation (1) essentially expresses, that there exists a lower limit for the motor volume for a given power output P. To avoid an over-heating of the rotor the losses P_{Rotor} due to electrical currents and electromagnetic fields have to be dissipated. In the case of air-cooling the heat is transfered from the rotor through the air gap to the stator, and the maximum admissible rotor losses are bounded by

$$P_{Rotor} \leq DL / (\pi\, \alpha\, \Delta T) \tag{2}$$

where ΔT is the temperature difference between rotor and stator and α is the heat transfer factor [6]. Another critical aspect is the vibrational behaviour of the rotor. From a rotordynamics point of view the bending eigenfrequencies of the rotor, which are considerably affected by the motor dimensions, should be kept as high as possible. Let's assume for an estimate of the first bending eigenfrequency that the total mass m of the motor, consisting of homogeneous material of the density ρ, is placed in the middle of the rotor shaft. The motor lamination is only considered as additional mass and does not influence the stiffness c of the rotor shaft. With the diameter ratio $\mu = d/D$, where d is the shaft diameter, the following equation for a rough estimate of the first bending eigenfrequency results:

$$\omega_R = \sqrt{c / m} = \sqrt{(3\, \mu^4 E\, D^2) / (\rho\, L^4)} \tag{3}$$

A comparison of equations (1) to (3) shows that the motor diameter D is the only parameter, which can simultaneously satisfy the requirements on power and dynamics. This means that an increase in the motor diameter leads to higher values for the achievable power output, higher rotor losses can be admitted, and bending eigenfrequencies will be higher. From the electrical as well as the mechanical point of view a large motor diameter is advantageous and the diameter should therefore be maximized. However, there are physical limitations as the maximum admissible motor diameter is limited because of centrifugal forces. In the case of a *rotating axisymmetric ring with a concentric borehole* the maximum circumferential velocity at which the yield strength σ_S is exceeded can be determined [3] and is given by:

$$v_{Max} = \frac{D_{Max}}{2}\, \omega = \sqrt{\frac{4\, \sigma_s}{\rho\, [(1 - \nu)\, \mu^2 + (3 + \nu)]}} \tag{4}$$

If ordinary transformer sheets are used (σ_S = 400 N/mm, ρ = 8 g/cm^3 and ν = 0.3) and if a diameter ratio μ = 0.5 is assumed, the yield strength of a rotating ring is exceeded at a circumferential velocity of 239 m/s. For *lamination sheets of induction motors*, which are weakened by slots and also have to carry the embedded squirrel-cage additional to their own weight, a circumferential velocity of about **200 m/s** is to be considered as an upper limit.

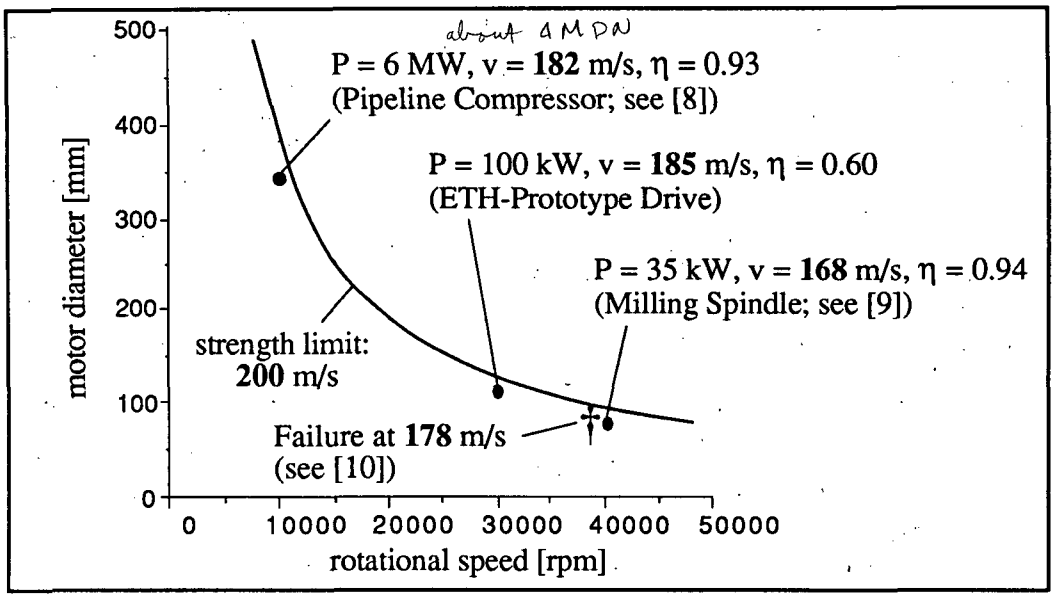

Figure 2: Maximum motor diameter in function of the rotational speed, with examples of some actual high speed drives ($\eta = \omega/\omega_R$ is the ratio of the rotation frequency to the first bending rotor eigenfrequency)

Figure 2 shows the corresponding admissible motor diameter in function of the rotational speed. For comparison the values for some actual high speed drives with different specifications and for different applications are included in the diagram. As one can see the maximum admissible motor diameter is decreasing inversely proportional to the rotational speed. Therefore with high operating speeds it becomes more and more difficult to attain high motor power outputs, to dissipate rotor losses and to stay below the first bending eigenfrequency of the rotor. As a consequence of these design limitations high speed drives often operate at the limits of feasibility and very close to the strength limit. This is confirmed by regarding the ratings of the realized machines included in Figure 2.

STRENGTH CALCULATION OF ELECTRIC HIGH SPEED DRIVES

Electric high speed drives often operate close to the strength limit and therefore the strength calculation of the motor unit, which usually is to be considered as the weak point of the rotor, is of primary importance. The lamination of the motor due to the slots (Figure 1) cannot be considered as an axisymmetric body. Therefore, in contrast to the axisymmetric lamination of magnetic bearings for example, the stresses cannot be determined by an analytical closed form solution. In addition, in the contact areas between transformer sheet and squirrel-cage nonlinear boundary conditions have to be taken into account. Last but not least, in order to locate areas where the yield stress might be exceeded material nonlinearities have to be considered. The *finite element method* is a very effective tool for the solution of such complex engineering problems, since arbitrary geometries and nonlinearities can be considered. In the following the nonlinear finite element analysis of the drive which failed at a circumferential velocity of about 178 m/s (Figure 2) will be summarized; see also [10]. On the left of Figure 3 the finite element model of the drive is shown. To save computing time only the smallest symmetrical segment of the motor cross-section as shown in Figure 1 was selected. The model consists of two separate bodies with different material and physical properties. For the lamination ordinary transformer sheets were used which were modeled with plane stress elements. For the squirrel-cage, which is made of aluminium, plane strain elements were used. For both bodies elastic-perfectly-plastic material behavior was

assumed, i.e. work hardening was not considered. The boundary conditions were chosen so that the nodes which are situated on the symmetry lines can only move along that line. It should be emphasized that the two bodies are completely separated by a very small air gap. For the resulting contact problem leading to nonlinear boundary conditions special analysis tools are provided by the finite element program which was used for the simulation [4].

In the middle of Figure 3 the computed equivalent von Mises stress at 34'000 RPM is shown. It can be seen that there is an abrupt change of stresses at the contact areas between transformer sheet and squirrel-cage which indicates that the nonlinear boundary conditions were considered adequately. In the transformer sheet, which is stressed much more than the squirrel-cage, the yield stress of 400 N/mm^2 is already reached, leading to two plastic zones at the inner area. As a result of this simulation study a failure could be explained that had occured during experiments with this high speed drive. By further increasing the rotation speed, up to 35'000 RPM, the plastic zones grow and finally the two initially separate zones meet, thus leading to a failure due to complete plastification of the carrying lamination area. Since work hardening was neglected in the simulation study this result is in good agreement with the experimental failure speed of about 38'000 RPM. The failure of the drive may be prevented by using a suitable slot geometry. For open slots the outer area of the transformer sheet is hardly stressed since tangential forces cannot be transfered. Therefore if the slot is closed the stress is more equally distributed and thus the material strength is better exploited (see Figure 3 on the right). For the transformer sheet with closed slots yield strength was firstly exceeded at 38'000 RPM in the simulation. As a consequence of these results for the ETH-high speed drive closed slots were used. A disadvantage of this approach is that closed slots lead to an undesired rise of the stray-field. However, by minimizing the thickness of the relevant cross-section the stray-field can be reduced strongly. For further considerations regarding the mechanical design of electric high speed drives refer to [11].

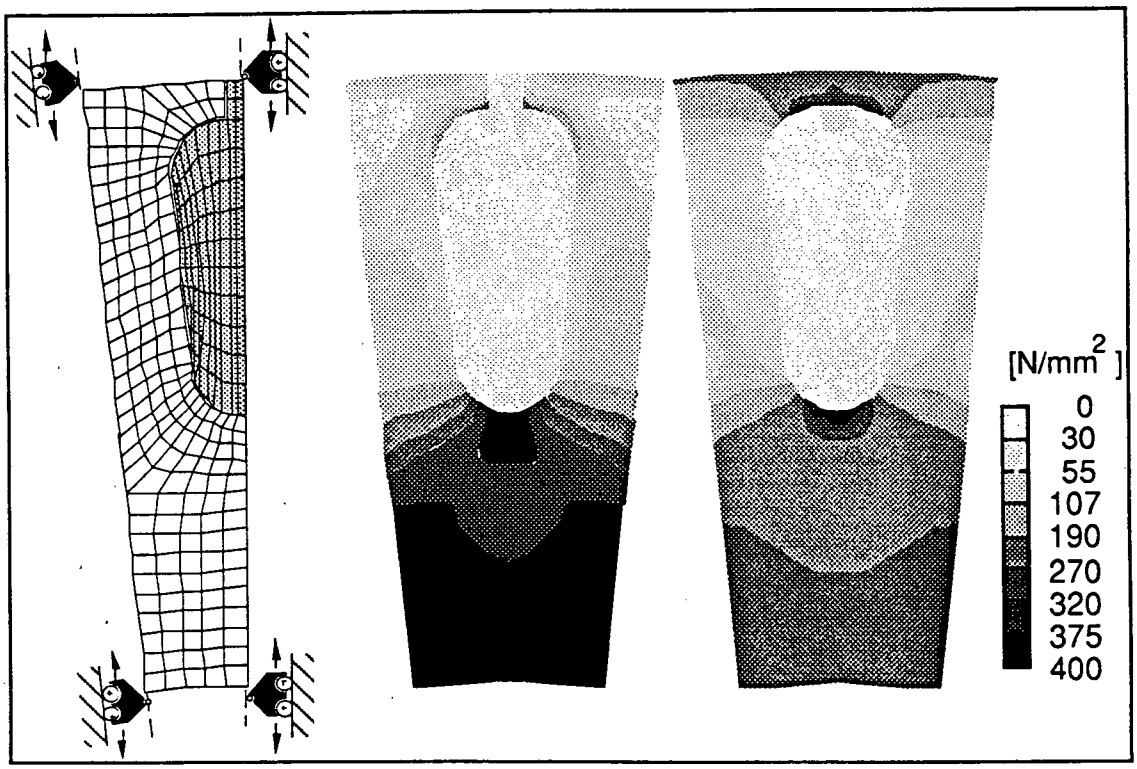

Figure 3: Finite element model of the motor cross-section with parts of the transformer sheet and the squirrel-cage (dark area) and equivalent von Mises stress at 34'000 RPM for open (in the middle) and closed slots (on the right).

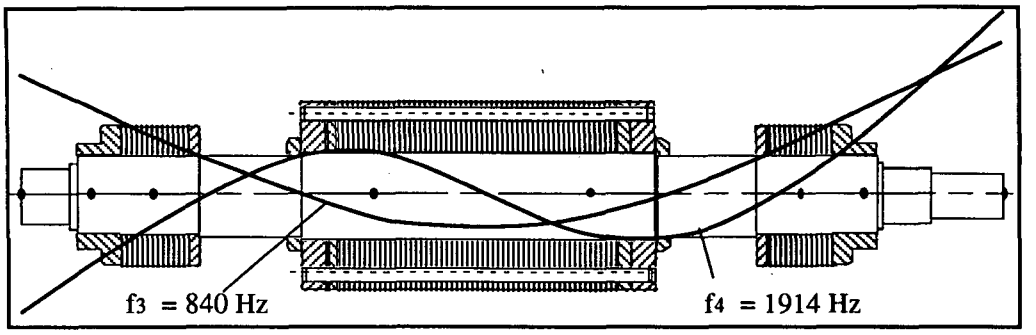

Figure 4: Shape and eigenfrequency of the 1st and 2nd elastic mode of the prototype rotor with motor-unit in the middle and magnetic bearings on the sides

MODELING OF THE ELASTIC HIGH SPEED ROTOR

The knowledge of the dynamic behavior of magnetically supported high speed rotors is necessary for the controller design. In this section the main conclusions on the modeling of the prototype high speed rotor are discussed. A detailed description of the modeling procedure can be found in [11]. Figure 4 shows the results for a first model of the prototype high speed rotor, obtained using a program specially adapted for rotordynamics and based on the exact solution of beam elements [5]. According to the usual modeling procedure the rotor is divided in a finite number of beam (i.e. rotor) elements which are connected together through the nodes located at the ends of each beam element. The effect of shrink-fitted lamination for the motor and the magnetic bearings on the rotor stiffness was considered in the simulation and adjusted with respect to the experimental results. To identify rotordynamics an experimental modal analysis was performed for the prototype rotor [2]. Figure 5 shows the frequency response measured at the right sensor ring for frequencies up to 3'200 Hz. For the two bending eigenmodes measured at 847 Hz and at 1896 Hz experiment (Figure 5) and simulation (Figure 4) show good agreement. However, there was an eigenmode identified at 990 Hz which was not predicted by the simulation. For the simulation the rotor was assumed to be axisymmetric, therefore one might guess that this effect was caused by orthogonal modes due to the finite number of slots or possibly unsymmetrical stresses resulting from the shrink-fit of the lamination. This was not the case, since the measured frequency difference of orthogonal modes was very small and further the "mysterious" mode at 990 Hz has it's own orthogonal mode. Next it was assumed that the effect may be caused by axial vibrations of the lamination or torsional modes.

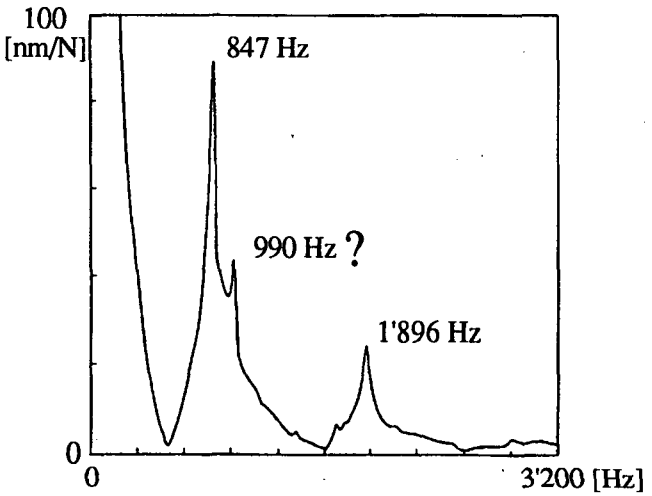

Figure 5: Measured frequency response of the prototype high speed rotor

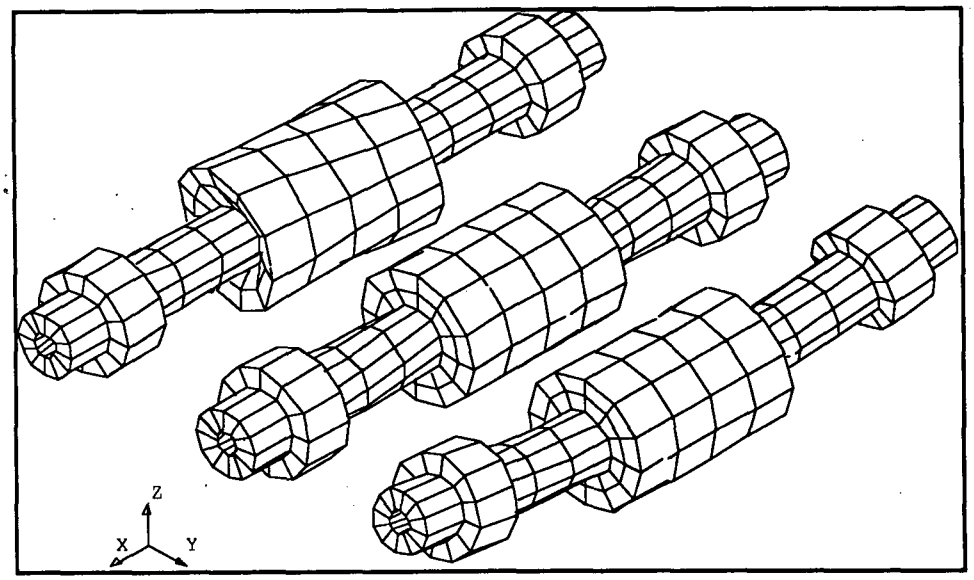

Figure 6: Results of 3-D FE-simulation, from left to the right: mode affecting motor lamination, torsional mode and bending mode

Therefore a three dimensional simulation of the rotor was made using a general purpose finite element program [4]. Additional modes caused by axial deflections of the lamination and torsional modes could be detected. However, as one can extract from Figure 6 these additional modes hardly affect bending and therefore it was concluded, that still some other mechanism must be responsible for the mode at 990 Hz. A calculation of the first bending eigenfrequency of the conductor bars fixed in the squirrel-cage finally gave the answer. For the 26 copper bars fixed in the squirrel-cage an eigenfrequency of 932 Hz resulted and therefore it was concluded that the squirrel-cage vibration was responsible for the "mysterious" mode at 990 Hz. These bars had been regarded as a non vibrating mass because they are embedded in the lamination. However, this embedding still leaves space for lateral displacements of the bars and leads to additional degrees of freedom for vibration. By regarding the 26 bars as an equivalent elastic beam and by an appropriate extension of the rotor model shown in Figure 4, the "mysterious" mode at 990 Hz finally could be modeled (see Figure 7). Now an adequate control of the AMB-system was feasible.

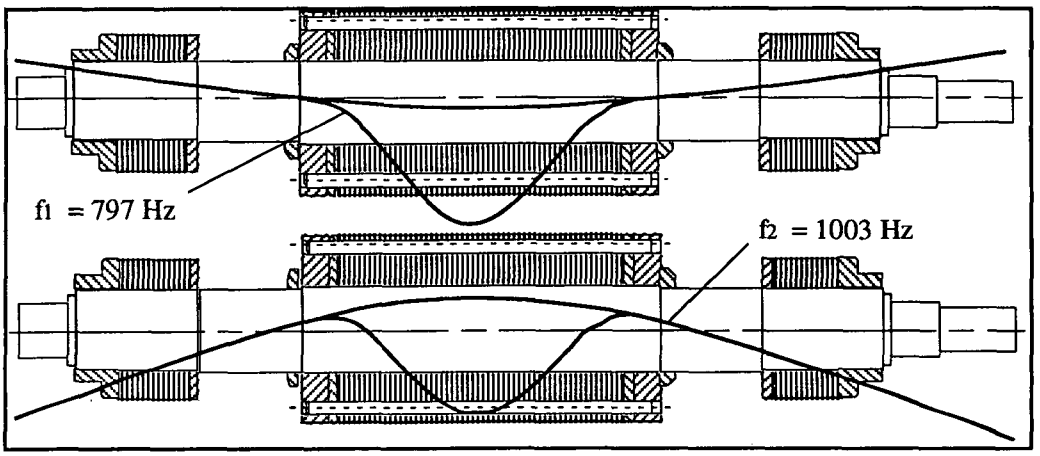

Figure 7: Shape and eigenfrequency of the 1st and 2nd elastic mode of the prototype rotor for the model regarding the squirrel-cage vibrations

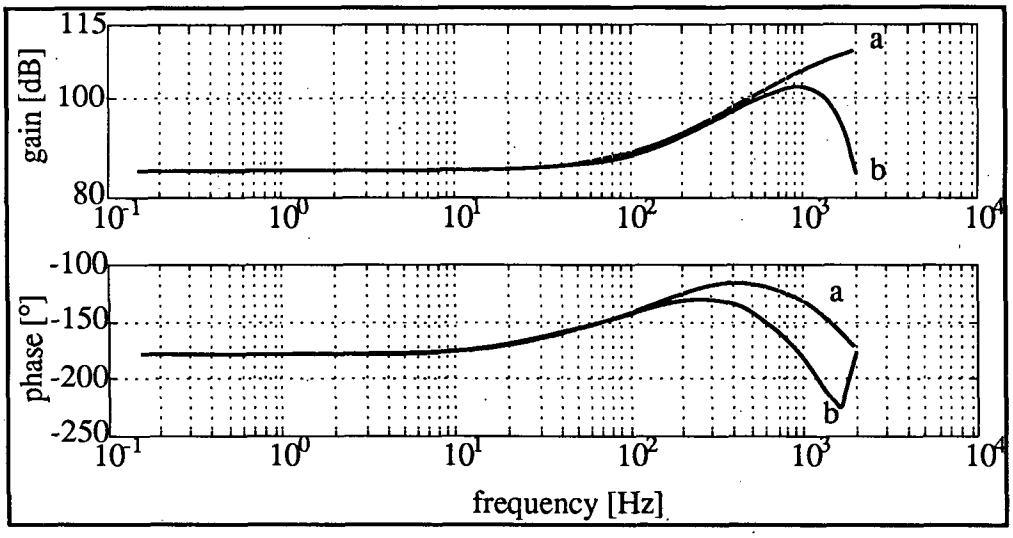

Figure 8: Bode plots of decentralized controllers of second (a) and fourth (b) order

DIGITAL CONTROL OF THE AMB-SYSTEM

An active damping of the elastic eigenmodes was not necessary for the prototype system since the rotor was designed stiff enough. Therefore the main controller task was to stabilize the open loop system and to allow a smooth operation up to the maximum speed of 30'000 rpm. The cut off frequency of the analog filter was fixed to 540 Hz. However, this cut off frequency turned out to be still high enough to make possible a destabilization of the elastic eigenmodes by the first controllers used for the prototype system; see also [11]. These problems could be overcome by using an adequate digital controller (Figure 8). In comparison to a similar controller of second order (a) the controller of fourth order (b) leads to low noise at high frequencies without deteriorating the controller dynamics at low frequencies. The decentralized controller of fourth order shown in Figure 8 was finally used for the prototype system.

As it was shown in the previous section the dynamics of the prototype rotor is strongly influenced by squirrel-cage vibrations. This effect vanishes with increasing rotational speed because the bars fixed in the squirrel-cage are pressed in the lamination by the centrifugal forces (at 30'000 rpm an acceleration of 52'668 g acts on the bars!). Therefore two models were regarded for the controller layout: model 1 with (Figure 7) and model 2 without (Figure 4) consideration of the squirrel-cage vibrations. The resulting eigenvalues of the open loop system and closed loop system for the controller finally used are shown in Table I.

The frequency response of the closed loop system excited by an unbalance is shown in Figure 9. According to the simulation the vibration amplitude becomes maximal near the second rigid body mode at 10'000 rpm and then decreases continuously up to 30'000 rpm.

TABLE I - EIGENVALUES OF THE OPEN AND CLOSED LOOP AMB-SYSTEM

	open loop	closed loop	
		model 1	model 2
rigid body mode	± 37	- 13 ± 65 Hz	- 13 ± 65 Hz
rigid body mode	± 57	- 33 ± 160 Hz	- 33 ± 160 Hz
1st elastic mode	- 14 ± 843 Hz	- 11 ± 840 Hz	- 6 ± 829 Hz
2nd elastic mode	- 15 ± 989 Hz	- 16 ± 980 Hz	--
3rd elastic mode	- 22 ± 1896 Hz	- 22 ± 1896 Hz	- 22 ± 1896 Hz

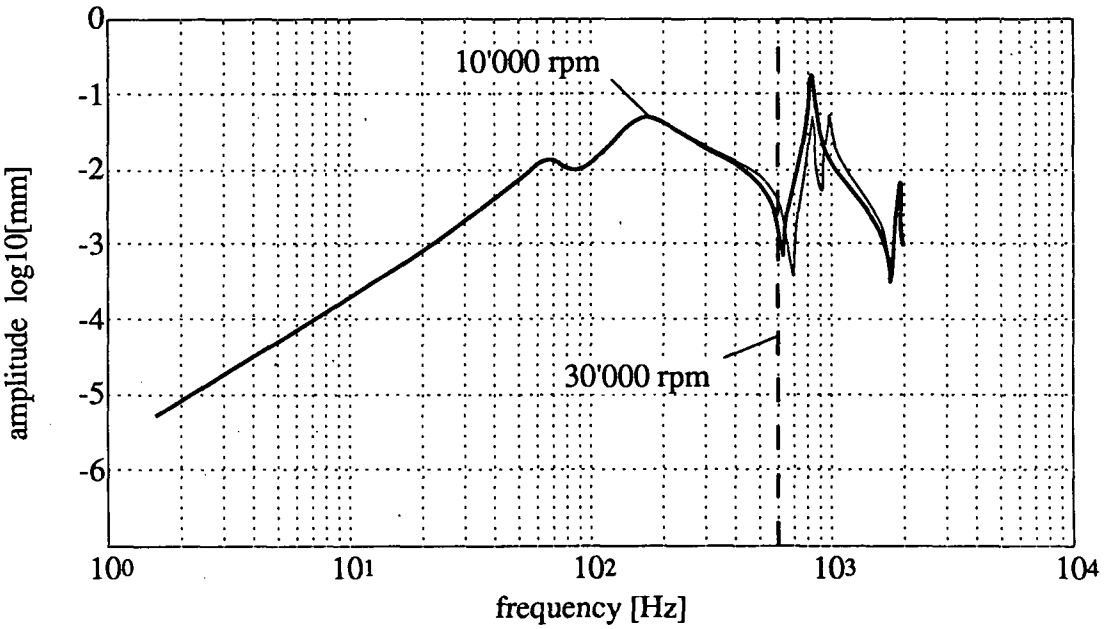

Figure 9: Simulated frequency response for an unbalance of 0.1 [kgmm] fixed at the bearing near the coupling. The bold line corresponds to the modell without and the thin line to the modell with consideration of the squirrel-cage vibrations.

REALIZATION OF THE ETH HIGH SPEED DRIVE SYSTEM

Figure 10 shows a cross-section of the ETH high speed drive with a power output of 100 KW and a rotational speed of 30'000 RPM. A noticeable feature of the prototype system is that the electric drive and the load are not acting on the same shaft. An arbitrary load can be coupled to the drive through the coupling device, and thus the system becomes more versatile. Even if there is some evident advantage of this modular approach, special care has to be taken to consider coupling effects. The axial load is determined by the kind of machine coupled to the drive, and therefore the axial bearing will have to be mounted on the load side. Thus the prototype drive is not equipped with an axial magnetic bearing. To attain sufficient machine cooling the jacket was provided with a cooling-water circuit. Additionally, the electric coils of the induction machine were filled with a heat conducting substance. Figure 11 shows the complete test stand for the ETH high speed drive. For the controller of the active magnetic bearings (AMB) a digital signal processor (DSP) system was used corresponding to the system described in [1]. Since power and frequency range of inverters for high speed power drives is limited by the capability of the electronic valves (thyristors, transistors) available, for the prototype machine a new modular voltage source inverter type was developed and realized [7]. Figure 12 finally shows the measured rotor displacement and the control current for 10'000 rpm and 30'000 rpm. As expected from the simulation (Figure 9) the deviations at 10'000 rpm are much larger than at 30'000 rpm.

CONCLUSIONS

In this paper a new generation of electric high speed drives was presented. For the realization of such drives new technologies as magnetic bearings or parallel switched inverters must be used and combined. Considerations concerning the design and the active magnetic support of the high speed rotor were made and a prototype system with 100 KW power and 30'000 RPM realized by the Mechatronics Lab was presented.

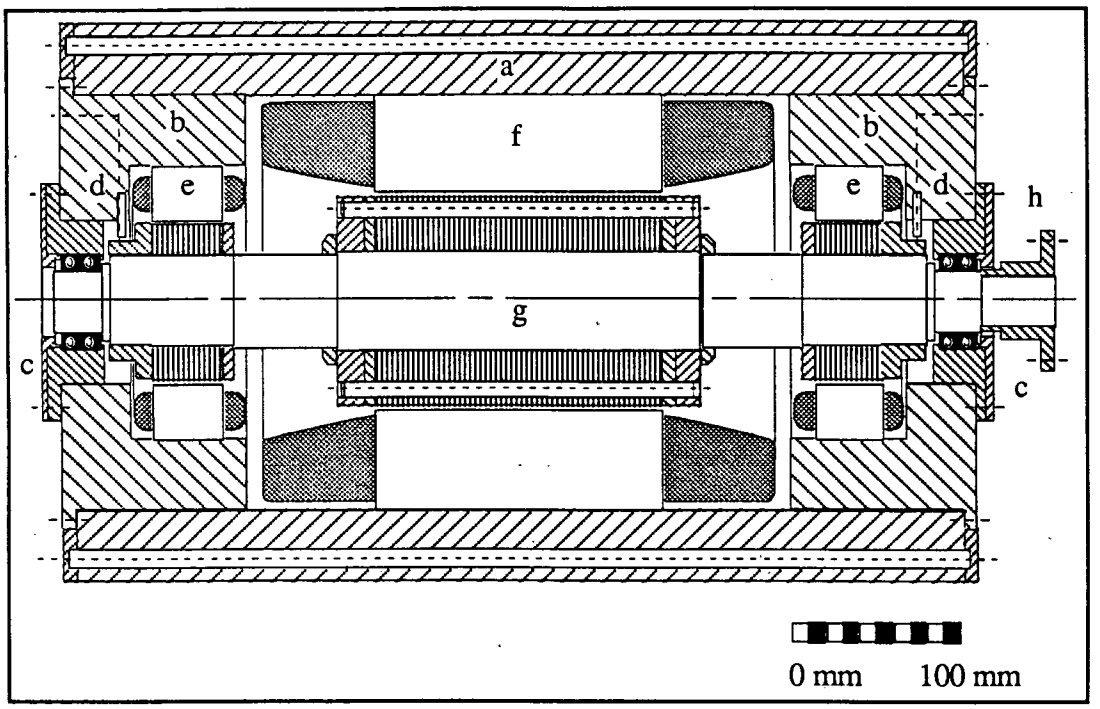

Figure 10: Cross-section of the magnetically supported high speed drive

a) watercooled jacket
b) bearing plate
c) backup bearing
d) displacement sensor
e) radial magnetic bearing unit
f) electric drive unit
g) rotor
h) coupling device

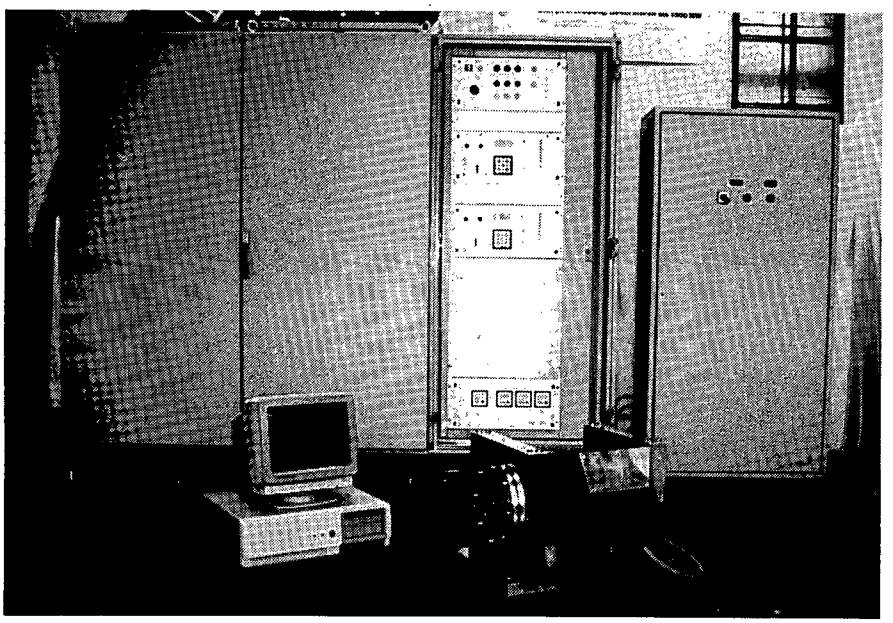

Figure 11: Complete electric high speed drive test stand with machine housing, PC containing digital controller hardware for the AMB-system, switched power amplifier for the magnetic bearings (rack on the right) and inverter for the electrical machine (other racks).

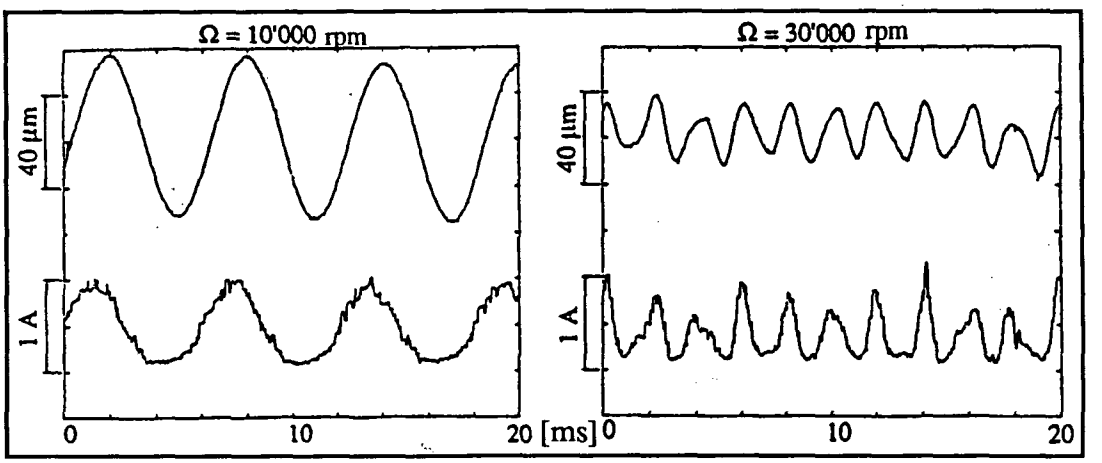

Figure 12: Measured rotor displacement and control current for the magnetic bearing near the coupling at 10'000 rpm and at the maximum speed of 30'000 rpm.

REFERENCES

[1] H. Bleuler, *"Controlling Magnetic Bearing Systems with a Digital Signal Processor"*, 1st International Symposium on Magnetic Bearings, ETH Zurich, Switzerland, June 1988.

[2] A. Frachebourg, F. Viggiano, *"Modalanalyse eines schnellen Antriebsrotors"*, Measurement report, IWF and IFR, ETH, Zurich, 1991.

[3] R. Larsonneur, *"Design and Control of Active Magnetic Bearing Systems for High Speed Rotation"*, Doct. Thesis ETH No. 9140, Zurich, 1990.

[4] MARC-MENTAT, *General-Purpose Finite Element Program*, Revision K4, Marc Analysis Research Corporation, Palo Alto, 1990.

[5] MADYN, *Hinweise zur Benützung des Programmpaketes*, Ingenieur-Büro Klement, Darmstadt, 1982.

[6] K. Reichert, P. Pasquarella, *"High Speed Electric Motor-Drives, Status, Trends and Problems"*, 15th FEE/ABINEE TEC'91, International Electro-Electronics Trade Fair, Sao Paulo, Brazil, 1991.

[7] R. Rohner, *"Schnelle Umrichter hoher Leistung mit parallelgeschalteten Einzelgeräten"*, Doct. Thesis ETH No. 9295, Zurich, 1990.

[8] J. Schmied, *"Experience with Magnetic Bearings Supporting a Pipeline Compressor"*, 2nd International Symposium on Magnetic Bearings, Tokyo, Japan, 1990.

[9] R. Siegwart, R. Larsonneur, A. Traxler, *"Design and Performance of a High Speed Milling Spindle in Digitally Controlled AMB's"*, 2nd International Symposium on Magnetic Bearings, Tokyo, Japan, 1990.

[10] F. Viggiano, *"Schadensanalyse eines Zerborstenen Schnellen Antriebes"*, VDI-Berichte 902, Düsseldorf, 1991.

[11] F. Viggiano, *"Aktive Magnetische Lagerung und Rotorkonstruktion Elektrischer Hochgeschwindigkeits-Antriebe"*, Doct. Thesis ETH, Zurich, to appear 1992